Electrochemistry in liquid sulfur dioxide. 3. Electrochemical production of new highly oxidized 2,2'-bipyridine complexes of ruthenium and iron

John G. Gaudiello, Paul R. Sharp, and Allen J. Bard

J. Am. Chem. Soc., **1982**, 104 (23), 6373-6377• DOI: 10.1021/ja00387a036 • Publication Date (Web): 01 May 2002

technique (at 2.8 Å resolution) ranged from 3.44 Å in metazidomyohemerythrin[32] to 3.05 Å in metaquohemerythrin.[4] It appears that it is going to be equally difficult to determine an accurate iron–iron distance with EXAFS. Hendrickson et al.[29] have EXAFS data indicating that the iron–iron separation in metazidohemerythrin is less than the 3.32-Å value for the oxo-bridged trimer $[Fe_3O(SO_4)_6(H_2O)_3]$. However, our EXAFS data (Table I) show that the iron–iron spacing in metazidohemerythrin is considerably longer than the 3.30 Å of the Fe(glycine) trimer. This discrepancy is outside our error limits, which are based on pairwise comparisons between hemerythrin, the Fe(Cl(PDC)) dimer, iron foil, and Fe(glycine) trimer. Further investigations are clearly needed to reconcile these differences.

Structure of Deoxyhemerythrin. The binuclear iron center of deoxyhemerythrin is shown also to possess octahedral iron coordination by the weakenss of the 3d pip in its near edge (Figure 2), in agreement with its near-infrared spectrum.[24] Furthermore, the histidine ligands from the protein backbone appear to be intact on the basis of the EXAFS peak from the third-shell atoms (Figure 4). However, the first-shell geometry is obviously quite different from the other forms. The EXAFS data indicate the loss of the μ-oxo bridge, in agreement with the observed lack of antiferromagnetic coupling between the irons in deoxyhemerythrin.[2] This loss is evident in three ways. The 3d pip in deoxyhemerythrin is smaller than in the ferric forms, consistent with the replacement around each iron of a single short bond by a more inversion-symmetric environment. More dramatic is the disappearance of the Fe–Fe peak in the transforms of Figure 4. Finally, the first-shell EXAFS data are different in the deoxy form from that of the other forms and from the Fe(Cl(PDC)) dimer.

The loss of the iron–iron peak in deoxyhemerythrin may indicate that there has been enough change in the distance of the iron atoms to cause the iron–iron signal to become buried under some other signal. This seems unlikely in view of the unaltered histidine EXAFS signal and the fact that crystals of deoxyhemerythrin can be converted to oxyhemerythrin without any change in crystal morphology.[31] Since the two iron atoms in hemerythrin are sandwiched between four α helices,[4] the 2-Å movement of the iron atoms required by this explanation would surely have caused a marked disruption in the polypeptide backbone orientation. An alternative explanation is that in the absence of the μ-oxo bridge the iron atoms undergo uncorrelated thermal vibrations that reduce the iron–iron signal to below the signal-to-noise ratio. Previous work on model compounds with multiple metal centers has indicated that metal–metal interaction is more likely to be detected by EXAFS when there is strong bridging between the metal atoms.[33] We plan to make more extensive measurements on deoxyhemerythrin as a function of temperature to test the above possibility. We will also attempt to find standards whose EXAFS more closely resemble that of deoxyhemerythrin and reserve our detailed analysis of the data until these experiments have been completed.

Conclusions

EXAFS measurements on deoxy-, oxy-, and methemerythrins have helped elucidate structural similarities and differences between them. There is now direct evidence that oxyhemerythrin has a similar structure to metazidohemerythrin and methydroxohemerythrin, differing in the nature of the bound anion. Although the iron–iron spacing from these measurements is somewhat longer than that measured by X-ray crystallography, the basic structure proposed by the latest crystallographic measurements[6] is supported. The data on deoxyhemerythrin show that while the histidine ligation has been retained, the EXAFS departs significantly from the other forms of hemerythrin. The iron–iron signal has disappeared, showing the loss of the bridging oxo group, and the first-shell distances other than the histidine nitrogen are rearranged.

Acknowledgment. We are pleased to acknowledge the advice and stimulating discusions with Drs. W. W. Parson, T. M. Loehr, R. E. Stenkamp, and L. H. Jensen. W.T.E. is indebted to James Collman, Eric Evitt, Bob Kreh, and Craig Barnes of the Stanford University Chemistry Department for assistance in handling oxygen-free samples. The research reported here was supported by the National Science Foundation (Grant PCM 79-03674) and the National Institutes of Health (Grant GM18865). The support and help of the staff of SSRL was essential in conducting these experiments. SSRL is supported by the National Science Foundation through the Division of Materials Research and the National Institutes of Health through the Biotechnology Resource Program in the Division of Research Resources in cooperation with the Department of Energy.

Registry No. Fe, 7439-89-6.

(32) Hendrickson, W. A.; Klippenstein, G. L.; Ward, K. B. *Proc. Natl. Acad. Sci. U.S.A.* **1975**, 2160–2164.

(33) Cramer, S. P.; Hodgson, K. O.; Stiefer, E. I.; Newton, E. W. *J. Am. Chem. Soc.* **1978**, *100*, 2748–2761.

Electrochemistry in Liquid Sulfur Dioxide. 3. Electrochemical Production of New Highly Oxidized 2,2′-Bipyridine Complexes of Ruthenium and Iron

John G. Gaudiello, Paul R. Sharp, and Allen J. Bard*

Contribution from the Department of Chemistry, The University of Texas at Austin, Austin, Texas 78712. *Received February 24, 1982*

Abstract: The electrochemical oxidation of $Ru(bpy)_3^{2+}$ and $Fe(bpy)_3^{2+}$ in liquid sulfur dioxide was investigated. $Ru(bpy)_3^{2+}$ shows two oxidation waves corresponding to the 3+ (1.01 V) and 4+ (2.76 V) forms while $Fe(bpy)_3^{2+}$ undergoes three oxidations to the 3+ (0.70 V), 4+ (2.92 V), and 5+ (~3.09 V) forms. While the 3+ form is stable for both compounds on a coulometric time scale, the higher oxidation states react with solvent to regenerate the 3+ form. The kinetics of this reaction was studied as a function of temperature by cyclic voltammetry, chronocoulometry, and chronoamperometry.

Introduction

Liquid sulfur dioxide containing a suitable electrolyte (e.g., tetra-*n*-butylammonium perchlorate, TBAP) has been shown to be a useful solvent for electrochemical studies, especially in the region of very positive potentials where strongly oxidizing species can exist.[1,2] Thus the limit for background oxidation with 0.1

0002-7863/82/1504-6373$01.25/0

M TBAP was estimated as ≃3.4 V vs. an aqueous saturated calomel electrode (SCE) by comparison of the potentials for oxidation of 9,10-diphenylanthracene (DPA) in SO_2 and acetonitrile. We report here the electrochemical oxidation of $Ru(bpy)_3^{2+}$ (bpy = 2,2′-bipyridine) to the 3+ and 4+ forms and $Fe(bpy)_3^{2+}$ to the 3+, 4+, and 5+ forms and data concerning the stability of these states in SO_2. The electrochemistry of $Ru(bpy)_3^{2+}$, $Fe(bpy)_3^{2+}$, and related compounds has been investigated in both protic and aprotic solvents.[3-8] While oxidation to the 3+ form is frequently observed, to our knowledge no more highly oxidized species have been reported.

Experimental Section

Electrochemical studies were carried out in conventional one- and three-compartment cells using previously reported experimental procedures.[1a] $[Ru(bpy)_3](PF_6)_2$ was prepared by refluxing *cis*-$(bpy)_2RuCl_2 \cdot 2H_2O$, prepared by published procedures,[9] with 1.2 equiv of bpy (Aldrich Chemical Co., Milwaukee, WI) in dimethylformamide under nitrogen. An excess of NH_4PF_6 was then added to precipitate the PF_6 salt. The resulting orange product was recrystallized from acetone/ether, washed with ether, and air-dried. $[Fe(bpy)_3](PF_6)_2$ was prepared by adding 3 equiv of bpy to an aqueous solution of $FeSO_4$. The PF_6 salt was obtained by adding NH_4PF_6. The red product was recrystallized from acetone/ether, washed with ether, and dried in vacuo. The supporting electrolyte, tetra-*n*-butylammonium fluoroborate ((TBA)BF_4, polarographic grade, Southwestern Analytical Chemicals, Austin, TX) was recrystallized three times from acetone/ether and vacuum-dried for 72 h. Tetra-*n*-butylammonium hexafluorophosphate ((TBA)PF_6) was prepared by adding equal molar amounts of tetra-*n*-butylammonium iodide (Southwestern Analytical Chemicals, Austin, TX) and NH_4PF_6 (Ozark-Mahoning) to acetone. NH_4I was removed by filtration, and (TBA)PF_6 was precipitated with water. The product was recrystallized first from hot ethanol and then from acetone/ether.

All electrochemical measurements were made with a Model 173 potentiostat, employing positive feedback for *iR* compensation, a Model 175 universal programmer, and a Model 179 digital coulometer (Princeton Applied Research Corp., Princeton, NJ). Current–voltage curves for scan rates less than 500 mV/s were recorded on a Model 2000 X-Y recorder (Houston Instruments, Inc., Austin, TX). Chronoamperometric and cyclic voltammetric data at scan rates greater than 500 mV/s were recorded with a Model 3001 processing digital oscilloscope (Norland Corp., Fort Atkinson, WI). Numerical integration of current transients with the digital oscilloscope yielded the chronocoulometric results. All potentials in this work are reported against an Ag quasi-reference electrode (AgRE) of a type previously described;[1a] this has a potential equivalent to ~+0.3 V vs. SCE. Visible absorption spectra were obtained with a Model 1250 optical multichannel analyzer (Princeton Applied Research Corp., Princeton, NJ) with a holographic grating (150 lines/mm) and a xenon lamp source.

Results

Background Limits. The anodic background limit for SO_2, 0.1 M TBAP, at a Pt electrode occurs at +2.4 V vs. AgRE and has been attributed to oxidation of perchlorate ion.[10] Thus the useful working range of the solvent should be extended to more positive potentials if anions more difficult to oxidize than perchlorate are employed. Two such anions are BF_4^- and PF_6^-. The anodic limit of SO_2 containing either (TBA)BF_4 or (TBA)PF_6 as supporting electrolyte is extended by another 0.6 V. This potential limit probably represents the oxidation of SO_2 itself, since the same positive limit is obtained whether (TBA)BF_4, (TBA)PF_6 or tetra-*n*-butylammonium fluoride is used.

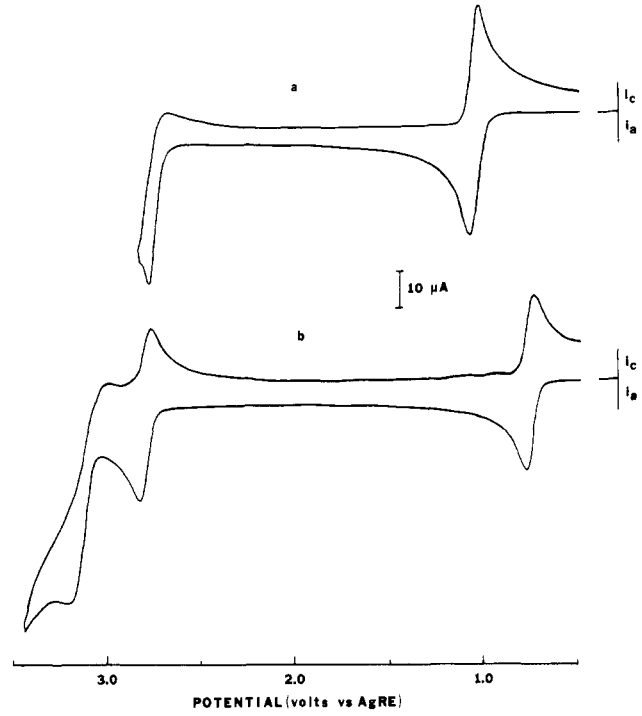

Figure 1. Cyclic voltammograms of (a) 4.7 mM $Ru(bpy)_3^{2+}$ in liquid SO_2 0.10 M (TBA)BF_4, at −40 °C with a scan rate of 100 mV/s and (b) 4.0 mM $Fe(bpy)_3^{2+}$ in liquid SO_2, 0.10 M (TBA)PF_6, at −70 °C, with a scan rate of 500 mV/s.

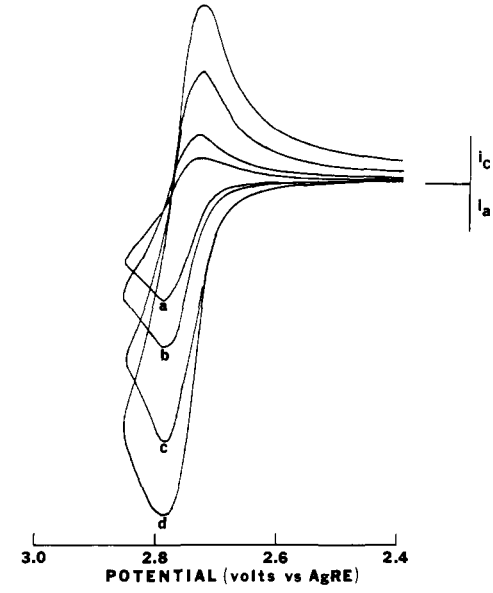

Figure 2. Effect of scan rate on the $Ru(bpy)_3^{3+/4+}$ couple (6.4 mM) at −40 °C and 0.10 M (TBA)BF_4: (a) 1 V/s; (b) 2 V/s; (c) 5 V/s; (d) 10 V/s.

Oxidation of $Ru(bpy)_3^{2+}$. A typical cyclic voltammogram for the oxidation of $Ru(bpy)_3^{2+}$ at a Pt-disk electrode is shown in Figure 1a. The first wave with an anodic peak potential, E_{pa}, of 1.03 V corresponds to a Nernstian one-electron, electrochemically reversible process. The difference between the cathodic and anodic peak potentials, $\Delta E_p = E_{pa} - E_{pc}$, is 48 mV, which corresponds closely to the expected value for a Nernstian wave at −40 °C (44 mV). Controlled-potential coulometry (CPC) carried out at 1.50 V gave an n_{app} value (faradays/mole of reactant consumed) of 0.99; the resultant light blue solution of $Ru(bpy)_3^{3+}$ was stable on the time scale of the experiment (~5 h).

The second oxidation wave shown in Figure 1a, E_{pa} = 2.78 V, corresponds to a second, one-electron oxidation. The $Ru(bpy)_3^{4+}$ species is not stable at v = 100 mV/s as shown by the presence

(1) (a) Tinker, L. A.; Bard, A. J. *J. Am. Chem. Soc.* **1979**, *101*, 2316. (b) Tinker, L. A.; Bard, A. J. *J. Electroanal. Chem. Interfacial Electrochem.* **1982**, *133*, 275 and references therein.
(2) Dubois, J. E.; Delamar, M.; Lacaze, P. C. *Electrochim. Acta* **1980**, *25*, 429.
(3) Tokel, N. E.; Hemingway, R. E.; Bard, A. J. *J. Am. Chem. Soc.* **1973**, *95*, 6582.
(4) Tanaka, N.; Sato, Y. *Electrochim. Acta* **1968**, *13*, 335.
(5) Falqui, M. T. *Gazz. Chim. Ital.* **1958**, *88*, 97.
(6) Saji, T.; Aoyagui, S. *J. Electroanal. Chem. Interfacial Electrochem.* **1975**, *58*, 401.
(7) Saji, T.; Aoyagui, S. *J. Electroanal. Chem. Interfacial Electrochem.* **1975**, *60*, 1.
(8) Saji, T.; Aoyagui, S. *J. Electroanal. Chem. Interfacial Electrochem.* **1975**, *63*, 31.
(9) Sullivan, B. P.; Salmon, P. J.; Meyer, T. J. *Inorg. Chem.* **1978**, *17*, 3334.
(10) Castellonese, P.; Lacaze, P. C. *C. R. Hebd. Seances Acad. Sci., Ser. C Acad. Sci.* **1972**, *274*, 2050.

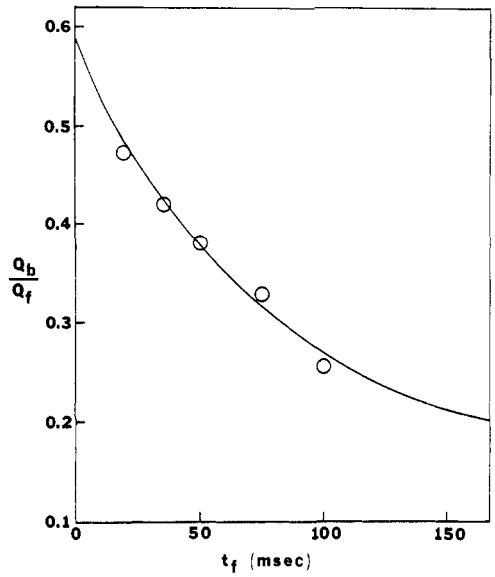

Figure 3. Plot of Q_b/Q_f vs. t_f for chronocoulometry. The solid line is theoretical results for $k = 12\ s^{-1}$. Points represent experimental data for $Ru(bpy)_3^{3+/4+}$ in 0.1 M $(TBA)BF_4$.

of only a small cathodic wave upon potential reversal. The effect of sweep rate on the CV waves for the $Ru(bpy)_3^{3+/4+}$ couple is shown in Figure 2. For $v \geq 5$ V/s at −40 °C the electrogenerated 4+ species is stable on the time scale of the experiment. At these high scan rates the couple exhibits Nernstian behavior and an $E^{0\prime}$ value (taken as the average of the anodic and cathodic peak potentials) of 2.76 V.

At low scan rates such as those of Figure 1a the i_{pa} value of the second (3+ → 4+) wave is larger than that of the first (2+ → 3+). This behavior is characteristic of a catalytic reaction, where the electrogenerated species reacts with a nonelectroactive one to regenerate the starting material (eq 1 and 2). The occurrence of such a catalytic reaction is also clear from controlled-potential coulometric oxidation of a 17 mM $Ru(bpy)_3^{3+}$ solution at 2.85 V. After three times the number of coulombs needed for complete oxidation for a one-electron process has passed, the solution remained light blue and its voltammetric behavior was essentially identical with that obtained for the original $Ru(bpy)_3^{3+}$ solution. The current during coulometry did not decay to background levels but rather remained constant throughout the experiment. Isolation of the compound after coulometry and dissolution in MeCN gave a green solution. Cyclic voltammetric studies on this solution showed a reversible one-electron reduction wave at 1.29 V vs. SSCE corresponding to the $Ru(bpy)_3^{3+/2+}$ couple.

$$Ru(bpy)_3^{3+} \rightleftarrows Ru(bpy)_3^{4+} + e^- \quad (1)$$

$$Ru(bpy)_3^{4+} + Z \rightarrow Ru(bpy)_3^{3+} + Y \quad (2)$$

To gain additional information about the kinetics of this following catalytic reaction, we employed double-potential-step chronocoulometry.[11] If the reaction obeys pseudo-first-order kinetics, i.e., Z in eq 2 is present in large excess, then a chemical rate constant can be determined from the ratio Q_b/Q_f (where Q_f and Q_b are the number of coulombs for oxidation and reduction, respectively) as a function of time for the forward step, t_f. Representative results, shown in Figure 3, show good agreement to the catalytic mechanism. Rate constants obtained from such studies are listed in Table I. An Arrhenius plot (ln k vs. $1/T$) is linear (Figure 4) and yields an activation energy of 12.8 kcal/mol. We believe that the solvent is the species that is oxidized in reaction 2 ($Z = SO_2$) because the rate constant was independent of supporting electrolyte concentration over a range of 0.1–0.3 M and the 4+/3+ oxidation occurs near the solvent limit. This implies that the oxidation of SO_2 is kinetically slow at the Pt electrode surface (i.e., occurs with a significant overpotential) but is catalyzed by the $Ru(bpy)_3^{4+/3+}$ couple. Similar reactions have been observed with other highly oxidized species such as those derived from oxidation of $Fe(bpy)_3^{3+}$ as discussed below.

Table I. Catalytic Rate Constants for $M(bpy)_3^{4+}$ Species

$Ru(bpy)_3^{4+}$		$Fe(bpy)_3^{4+}$	
temp, °C	rate const, s^{-1}	temp, °C	rate const, s^{-1} [a]
−60	0.87	−38	0.1
−54	2.4	−32	0.3
−50	2.7	−26	0.4
−45	11	−22	0.6
−40	12	−15	1.6
−35	23		
−30	33		

[a] Average of CV and chronoamperometric results.

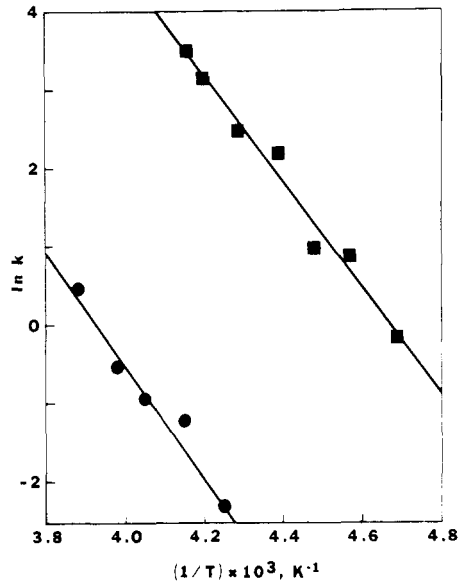

Figure 4. Arrhenius plot, ln k vs. $1/T$, for the catalytic reaction $M(bpy)_3^{4+} + Z \xrightarrow{k} M(bpy)_3^{3+} + Y$, where $k = k_c[Z]$: (■) $Ru(bpy)_3^{4+}$; (●) $Fe(bpy)_3^{4+}$.

Oxidation of $Fe(bpy)_3^{2+}$. A typical CV observed for the oxidation of $Fe(bpy)_3^{2+}$ in SO_2 is shown in Figure 1b. The first wave ($E_{pa} = 0.76$ V) corresponds to a reversible one-electron oxidation. Controlled-potential coulometry at 1.0 V gave $n_{app} = 0.97$. The dark blue solution of $Fe(bpy)_3^{3+}$ was stable for at least 4 h at temperatures up to −15 °C. Two other oxidation waves are observed at 2.88 and 3.14 V in both the $Fe(bpy)_3^{2+}$ and the electrogenerated $Fe(bpy)_3^{3+}$ solutions. At higher scan rates (≥10 V/s) the wave at 2.88 V corresponds to the Nernstian one-electron reaction (3); whereas the wave at 3.14 V corresponds to the quasi-reversible, one-electron reaction (4). At lower scan rates

$$Fe(bpy)_3^{3+} \rightleftarrows Fe(bpy)_3^{4+} + e^- \quad (3)$$

$$Fe(bpy)_3^{4+} \rightleftarrows Fe(bpy)_3^{5+} + e^- \quad (4)$$

instability of both the 4+ and 5+ forms is observed, again probably caused by a catalytic reaction with SO_2. The kinetics of this reaction were studied by CV[12] and chronoamperometry.[13]

Chronoamperometric data were obtained by stepping the potential of a Pt electrode in a 4 mM $Fe(bpy)_3^{3+}$ solution 100 mV beyond E_{pa} for reaction 3 and monitoring the current as a function of time, t. For $t < 100$ ms the catalytic reaction had a negligible effect on the current responses and the i–t curve followed the

(11) Christie, J. H. *J. Electroanal. Chem. Interfacial Electrochem.* **1967**, *13*, 79.

(12) Nicholson, R. S.; Shain, I. *Anal. Chem.* **1964**, *36*, 706.

(13) Bard, A. J.; Faulkner, L. R. "Electrochemical Methods"; Wiley: New York, 1980; Chapter 11.

Table II. Summary of Voltammetric Parameters and Spectral Properties for Tris(2,2'-bipyridine) Complexes of Ruthenium and Iron in Liquid Sulfur Dioxide[a]

complex	E_{pa}, V	$E_{pa}-E_{pc}$, mV	$E^{\circ\prime}$, V	abs max, eV	molar abs M^{-1} cm^{-1}	$E^{\circ\prime}$(calcd), V[b]	$10^6 \times$ (diffusion coeff), cm^2/s
$Ru(bpy)_3^{2+}$	1.03	48	1.0 (3+/2+)	2.71	11900		2.8
$Ru(bpy)_3^{3+}$	2.78	49	2.76 (4+/3+)	1.83	407	2.84	
$Fe(bpy)_3^{2+}$	0.76	46	0.74 (3+/2+)	2.35	8660		2.0
$Fe(bpy)_3^{3+}$	2.83	92	2.80 (4+/3+)	2.01	284	2.75	
$Fe(bpy)_3^{4+}$	3.14	123	3.09 (5+/4+)				

[a] Ru data is for $T = -40$ °C, 0.1 M $(TBA)BF_4$; Fe data is for $T = -70$ °C, 0.1 M $(TBA)PF_6$, except for the diffusion coefficient, where $T = -40$ °C. $E^{\circ\prime}$ is taken as the average of the anodic and cathodic peak potentials. [b] From eq 9.

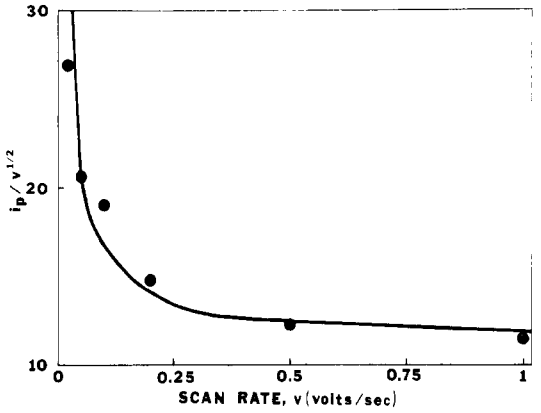

Figure 5. Plot of normalized anodic peak current, $i_p/v^{1/2}$, vs. scan rate, v, for $Fe(bpy)_3^{3+/4+}$. The solid line is theoretical results for $k = 1.6$ s^{-1}. Points represent experimental data at −15 °C, 0.13 M $(TBA)PF_6$.

expected Cottrell behavior.[13] From this short time data (5–100 ms), a value for the combined constant $AD^{1/2}C^*$ (where A is the area, D is the diffusion coefficient, and C^* is the bulk concentration) can be calculated from the slope of the i vs. $t^{-1/2}$ line. With this value the expected current response at longer times in the absence of kinetic perturbation, i_{diff}, can be calculated. A comparison of the measured catalytic current, i_k, to i_{diff} allows a rate constant to be determined.[13] The rate constants from cyclic voltammetric data were obtained in a similar fashion by comparing the ratio of the expected anodic peak current in the absence of a chemical reaction to those actually obtained for the $Fe(bpy)_3^{3+}$ system as a function of v.[12] At sufficiently large v, the electron-transfer reaction (3+ → 4+) is unperturbed by the following reaction and $i_{pa}/v^{1/2}$ is constant. At smaller v, $i_{pa}/v^{1/2}$ increases because of the regeneration of the 3+ form. The rate constant was calculated from plots of normalized i_{pa} vs. v (Figure 5). Results as a function of temperature are listed in Table I. The Arrhenius plot of these data (Figure 4) gave an activation energy of 13 kcal/mol.

Discussion

The standard potentials for the couples in SO_2 are listed in Table II. As discussed below, the oxidized forms (4+ and 5+) may be represented as a bpy radical cation coordinated to the 3+ metal center. This is analogous to the reduced forms of $Ru(bpy)_3^{2+}$, which have been represented as bpy^- coordinated to the 2+ metal.[4,6] Thus, reduction of $Ru(bpy)_3^{2+}$ and $Fe(bpy)_3^{2+}$ occurs with the addition of an electron to each bpy, resulting in three closely spaced waves corresponding to the 1+, 0, and 1− species.[3,6] The potentials for these reductions are relatively insensitive to the metal center.

The oxidation of the free ligand, bpy, in SO_2 occurs at +2.1 vs. AgRE. The wave shows no cathodic reversal current for scan rates up to 20 V/s, suggesting instability of the oxidized product. The actual thermodynamic potential for the bpy^+/bpy couple lies to more positive values, since a fast following irreversible reaction causes a negative shift of E_{pa}.[13]

Coordination of the bpy with the metal center probably makes its oxidation more difficult, consistent with the location of the

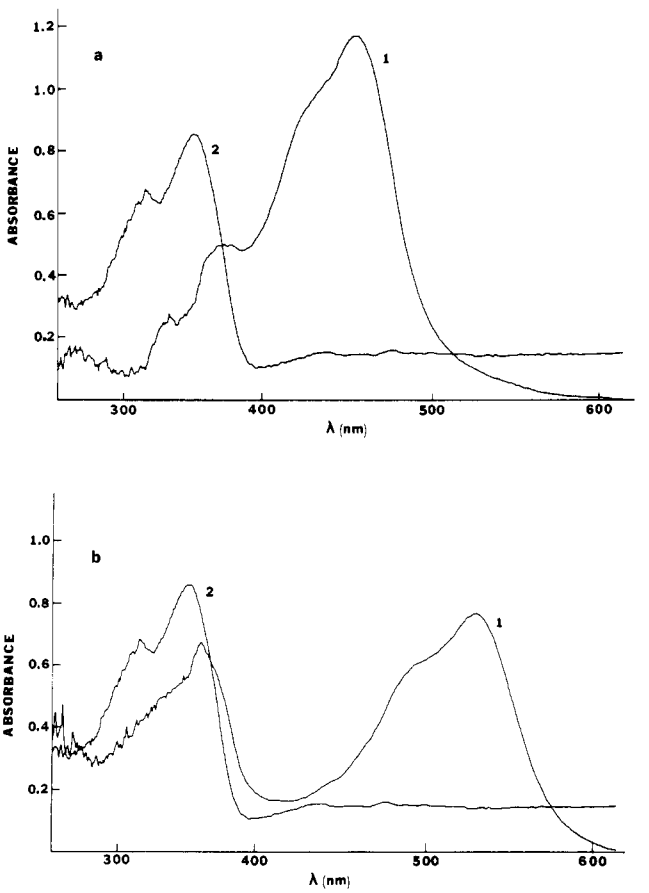

Figure 6. Absorption spectra of $Ru(bpy)_3^{2+}$ and $Fe(bpy)_3^{2+}$ in liquid SO_2, with path length 1 cm: (a) 9.87×10^{-5} M $Ru(bpy)_3^{2+}$ (1), liquid SO_2 (2); (b) 8.90×10^{-5} M $Fe(bpy)_3^{2+}$ (1) liquid SO_2 (2).

3+/4+ waves at 2.8 V vs. AgRE. Note that the waves for both the $Fe(bpy)_3^{3+/4+}$ and $Ru(bpy)_3^{3+/4+}$ couples occur at essentially the same potentials (in contrast to the situation for the 2+/3+ waves), consistent with the concept that this represents oxidation of a bpy. Additional evidence for this model is obtained from a joint consideration of the spectroscopic and electrochemical data, as proposed by Creutz, Sutin, and co-workers for reduction of bpy complexes.[14] Visible absorption spectra for both the bivalent and the tervalent complexes of Ru and Fe in liquid SO_2 are shown in Figures 6 and 7. The absorptivity and absorption maxima wavelengths, summarized in Table II, are similar to those reported in other solvents.[15,16] The spectrum of liquid SO_2 (uncorrected for reflective losses) shows an absorption maximum at 360 nm (Figure 5). Since the spectra for the complexes were obtained by digital subtraction of the background SO_2 spectrum from the

(14) Creutz, C. *Comments Inorg. Chem.*, in press.
(15) Bryant, G. M.; Fergusson, J. E. *Aust. J. Chem.* **1971**, *24*, 275.
(16) Bryant, G. M.; Fergusson, J. E.; Powell, H. K. J. *Aust. J. Chem.* **1971**, *24*, 257.

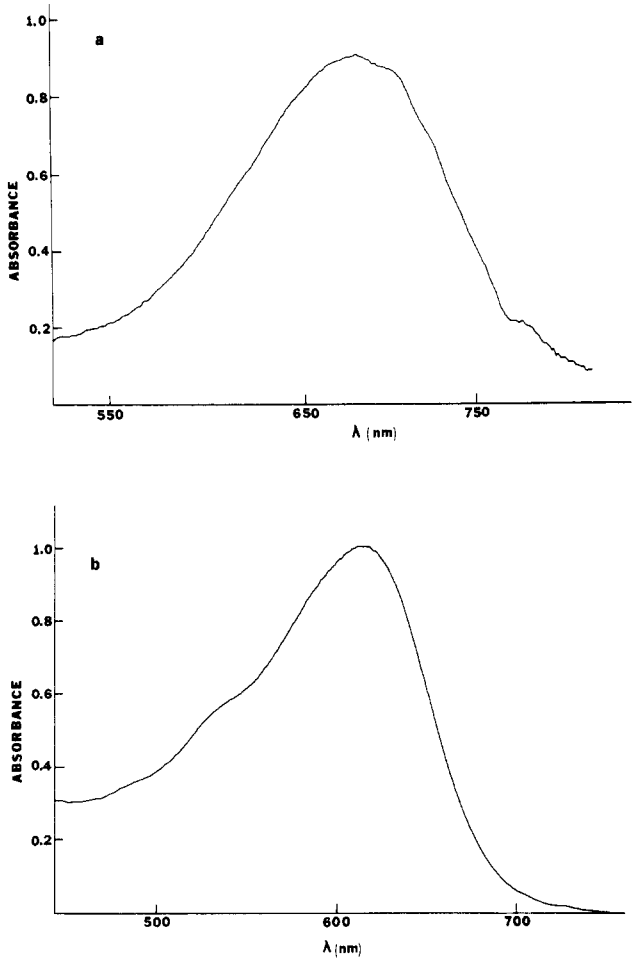

Figure 7. Absorption spectra of $Ru(bpy)_3^{3+}$ and $Fe(bpy)_3^{3+}$ in liquid SO_2, with path length 1 cm: (a) 2.24×10^{-3} M $Ru(bpy)_3^{3+}$; (b) 3.90×10^{-3} M $Fe(bpy)_3^{3+}$.

complex solution spectrum, the shorter wavelength portions of both the $Ru(bpy)_3^{2+}$ and the $Fe(bpy)_3^{2+}$ spectrum are distorted by the SO_2 absorption edge. The absorption band for $Ru(bpy)_3^{3+}$ and $Fe(bpy)_3^{3+}$ has been assigned to a $\pi \rightarrow t_{2g}$ transition, i.e., a ligand to metal charge transfer.[17] The redox potential for the 4+/3+ couple can be estimated from the energy of this transition and the potential for the 3+/2+ couple through the cycle given by eq 5–8. By combining reactions 5 and 6 the redox potential for

$$[M^{III}(bpy)_3]^{3+} + h\nu \rightleftarrows [M^{II}(bpy)_2(bpy^{+\cdot})]^{3+} \quad (5)$$

$$[M^{III}(bpy)_3]^{3+} + e^- \rightleftarrows [M^{II}(bpy)_3]^{2+} \quad E^\circ_{3+/2+} \quad (6)$$

$$[M^{II}(bpy)_2(bpy^{+\cdot})]^{3+} + e^- \rightleftarrows [M^{II}(bpy)_3]^{2+} \quad E^\circ_7 \quad (7)$$

$$[M^{III}(bpy)_2(bpy^{+\cdot})]^{4+} + e^- \rightleftarrows [M^{III}(bpy)_3]^{3+} \quad E^\circ_{4+/3+} \quad (8)$$

reaction 7 can be estimated ($E^\circ_7 = E^\circ_{3+/2+} + h\nu$). If it is assumed that the oxidation potential of bpy is not significantly affected by the charge on the metal center and if distortions between the ground and excited states are small, then the potential for oxidation of the 3+ species (eq 8) is given by

$$E^\circ_{4+/3+} = E^\circ_7 = E^\circ_{3+/2+} + h\nu \quad (9)$$

The values of $E^\circ_{4+/3+}$ calculated from $E^{\circ\prime}_{3+/2+}$ and the absorption spectrum of the 3+ species shown in Table II agree well with the experimental values of $E^{\circ\prime}_{4+/3+}$. The closely spaced 5+/4+ wave for the iron compound is also in agreement with this idea; a third oxidation wave is expected but would merge into the background oxidation of the solvent.

Conclusion

The large anodic window of SO_2 with $(TBA)BF_4$ or $(TBA)PF_6$ supporting electrolyte, equivalent to potentials up to ~+4 V vs. SCE, allows the electrochemical generation of transition-metal complexes in high oxidation states. Although catalytic reactions of these with SO_2 occur, the systems appear sufficiently stable, especially at lower temperatures, for characterization, e.g., by spectroscopic techniques, and studies such as these are under way. Preliminary studies involving complexes of first-, second-, and third-row transition metals have provided further examples of the utility of this solvent system for the production of highly oxidized materials. These results will be reported elsewhere.

Acknowledgment. The support of this research by the National Science Foundation (Grant No. CHE 7903729) is gratefully acknowledged. We are indebted to Drs. Norman Sutin and Carol Creutz (Brookhaven National Laboratory) for helpful suggestions and discussions concerning this work.

Registry No. $Ru(bpy)_3^{2+}$, 15158-62-0; $Fe(bpy)_3^{2+}$, 15025-74-8; $Ru(bpy)_3^{3+}$, 18955-01-6; $Fe(bpy)_3^{3+}$, 18661-69-3; $Fe(bpy)_3^{4+}$, 83207-86-7; $Ru(bpy)_3^{4+}$, 83207-87-8; $Fe(bpy)_3^{5+}$, 83207-88-9; SO_2, 7446-09-5.

(17) (a) Williams, R. J. *J. Chem. Soc.* **1955**, 137. (b) McCaffery, A. J.; Mason, S. F.; Norman, B. J. *J. Chem. Soc. A* **1969**, 1428.